Transactions of the TSME (2015) Vol. 3, No. 1, 7- 21
Journal of Research and Applications in Mechanical Engineering

ISSN 2229-2152 print
DOI: 10.14456/jrame.2015.1

Research Article

FLOW AND MIXING IN A MODEL SWIRL COMBUSTOR EQUIPPED WITH A TELESCOPIC END PLATE POROUS MEDIUM

S. Jugjai*
U. Praweenvisan
Y. Laoonual
Combustion and Engine Research Laboratory (CERL),
Department of Mechanical Engineering, Faculty of Engineering,
King Mongkut's University of Technology Thonburi (KMUTT),
126 Pracha Uthit Road, Bangmod, Thungkru,
Bangkok, 10140, Thailand

ABSTRACT:
This paper reports an experimental investigation of a non-reacting turbulent swirl flow in a transparent model swirl combustor equipped with a telescopic end plate porous medium (PM), in an effort to design and developing a future combustion system based on a concept of a PM burner. Focus has been made on characterization and optimization of flow fields and mixing performance within the model combustor under various burner geometries, which are characterized by the number of tangential inlet N_{inlet}, inlet angle ø and the inter-distance X_{PM} between the telescopic end plate PM and the air inlet nozzle. PIV (particle image velocimetry) flow visualization technique is employed to study the flow fields and the mixing performance in terms of averaged turbulence intensity. The flow fields show, how the flow velocities and structures vary as the controlling parameters vary. Based on the experimental results an optimum burner configuration is revealed. The relating parameters, in particular the telescopic end plate PM has a relatively large scale effect on flow fields and mixing phenomena.

Keywords: *Porous medium burner, swirl flow burner, mixing, turbulence intensity, PIV*

NOMENCLATURE

D	diameter	w	tangential components of the velocity
L	length	u'	velocity fluctuation in axial direction
N_{inlet}	number of the tangential inlet nozzles	v'	velocity fluctuation in radial direction
R	radius	X	axial position
Re	Reynolds number	X_{PM}	inter-distance
S	swirl number	Y, r	radial position
TI	turbulence intensity	ø	inlet angle
u	axial components of the velocity	Φ	equivalence ratio
v	radial components of the velocity	ν	kinematic viscosity
V	volume, or velocity magnitude	–	time averaging
Subscripts			
Avg	average	*mag*	magnitude
img	imaginary	*PM*	porous medium

* Corresponding author: S. Jugjai
E-mail address: sumrueng.jug@kmutt.ac.th

1. INTRODUCTION

In general combustion engineering, it is desirable to achieve complete mixing in the shortest possible length of a combustion (or mixing) chamber. To obtain the desirable short mixing length, a concept of "turbulence mixing" is adopted. The ability of a turbulent mixing system to mix two gases will depend upon the turbulence intensity, the scale of turbulence, the length of the mixing region and the velocity of the gas through the mixing system. By analogy with the familiar parameter "combustion intensity", the "mixing intensity" (I) is defined as the total mass of fuel and air mixed per unit time ($\dot{m}$), per unit volume (V), per unit density (ρ)

$$I = \dot{m}/V\rho = u/L = 1/\tau \tag{1}$$

Thus, the mixing intensity is equal to the reciprocal of the residence time τ. We need to determine the turbulence intensity (TI) which is one of the important factors controlling the mixing intensity. The higher the TI, the higher the mixing intensity with short residence time τ. TI reflects not only the mixing intensity but also the flow stability in the combustors, which has a significant effect on the subsequent combustion characteristics.

One effective method of producing high TI with a relatively short mixing length is by applying a swirl motion to the flow [1]. In a swirl flow, it is well known that the axial velocity decays very rapidly with distance [2, 3]. Further, the TI in the developed region is higher since, for a given axial velocity of the jet, there is an additional tangential velocity, representing an increase in the jet's kinetic energy. It follows that the reduction in the distance required to generate turbulence, with the greater amount of turbulence possible with vortex mixing systems, will significantly increase the over-all mixing intensity. Not only improvement in the mixing intensity but also favorable flame stabilization can be achieved by using the swirl flow. The utilization of swirl flow of air in burners has proven to be a powerful tool for control of mixing, flame stability, combustion intensity and efficiency [3].

With a recent development in a PM (porous medium) burner, it is successfully applied to burn liquid fuel (kerosene) without atomization [4-7]. Evaporation of the liquid fuel is achieved by a phase change phenomenon caused by a non-thermal equilibrium and a complex heat transfer between phases within the PM burner. Mixing between fuel vapor and air is achieved by a tangential injection of the air into the fuel vapor within a mixing chamber prior to combustion within the PM burner. In this regard, the mixing process of the fuel vapor and the air is of importance in view of combustion efficiency with low emission of pollutants. Detailed study of the mixing process is interesting and worthwhile for the design and development of a new combustion system of liquid fuel based on the concept of the PM burner.

To the authors' knowledge there have not been any reported studies on the flow field and mixing under non-reacting flow condition inside a transparent swirl model combustor equipped with a telescopic end plate PM using PIV (particle image velocimetry). The swirl flow is achieved via the use of a direct tangential entry of air into the model combustor, whereas fuel (gas or liquid) is fed through the telescopic end plate PM for controlling the mixing process between the fuel and the air. It should be emphasized here that the work presented in this article is an attempt to understand the fluid mechanics in relation to the telescopic end plate PM within the model combustor. The ultimate goal is to improve the design and to help develop strategies for controlling the mixing within a futuristic modular PM burner that can be operated under a partially premixed or a non-premixed flame mode with flexible fuels of liquid and gas. A parametric study of effects of dominating parameters affecting the turbulence intensity has been examined and optimized. An understanding of the highly turbulent features of the swirl flow motions inside the proposed swirl flow burner equipped with a telescopic end plate PM will shed a light on how to advance its combustion performance.

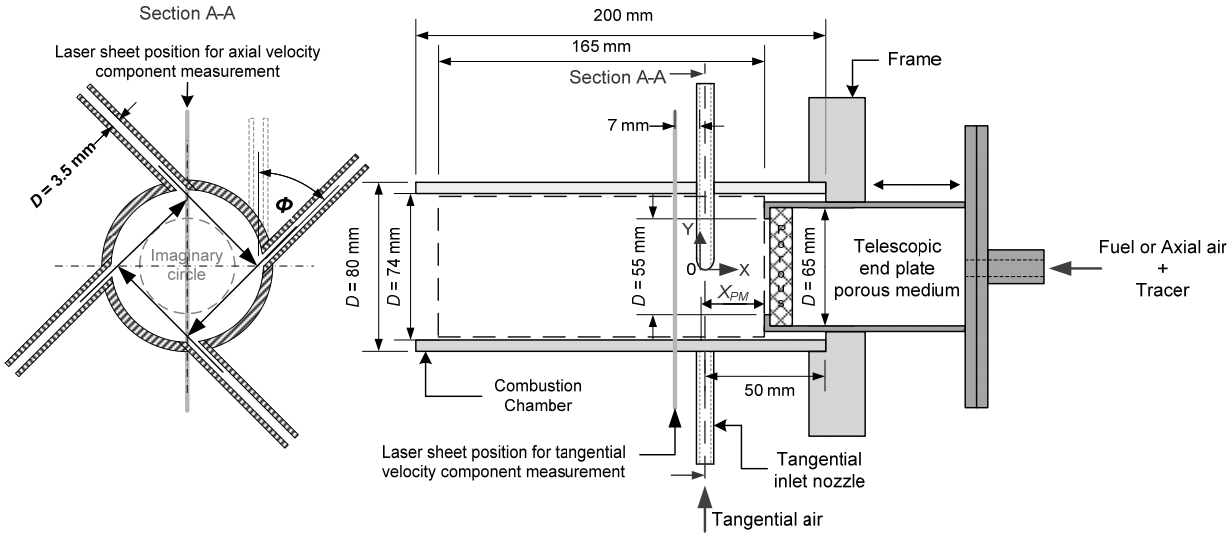

(a) test model combustor

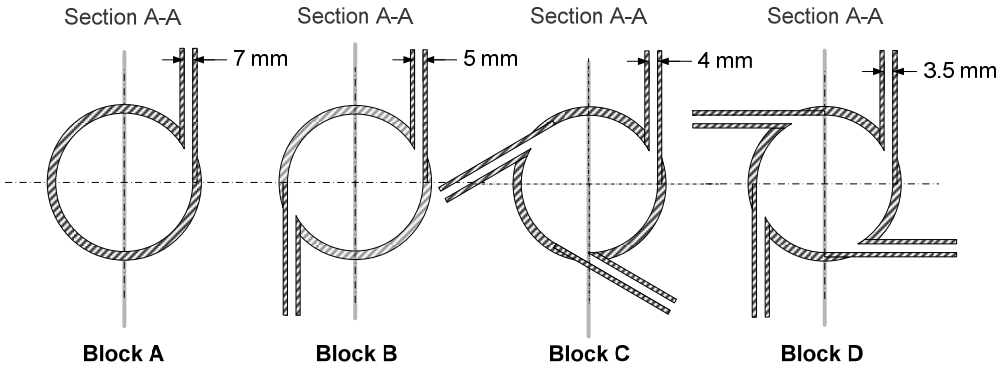

(b) Combustion chamber with varying N_{inlet}

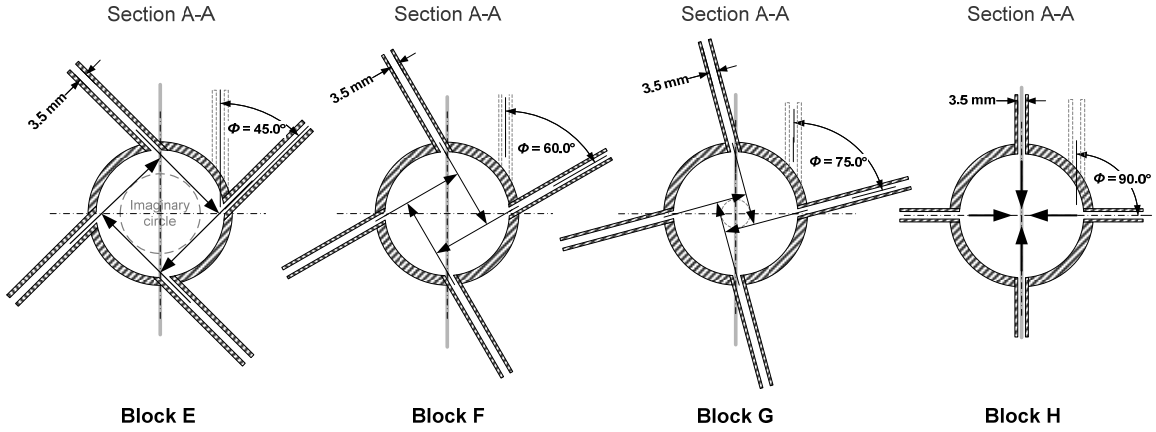

(c) Combustion chamber with varying ø

Fig. 1. Experimental setup.

2. EXPERIMENTAL SETUP

2.1 Test model combustor

Fig. 1a shows a schematic view of the test model combustor. All dimensions shown are in mm. It consists of two main components: a horizontal combustion chamber and a telescopic end plate PM, which are concentrically installed on the same frame. In general, the present burner looks similar to a type 1 cyclone combustor with tangential air supply [3]. However, they are different from each other in terms of the fuel supply and type of the burner end plate being installed. Gaseous fuel is premixed with the tangential air for the type 1 cyclone combustor, which is equipped with a solid end plate [3]. On the other hand, for the presently considered model combustor, a fuel (gas or liquid) is separately supplied through the combustor end plate, which is porous and telescopic. This telescopic end plate PM is very important in controlling mixing process between fuel and air as will be shown later.

The telescopic end plate PM is made of an acrylic cylinder with a stack of stainless screen wire mesh (with mesh size of 30 mesh/inch) installed inside at the exit end. This stainless screen wire mesh can make possible evaporation of the liquid fuel (kerosene) being supplied through it into fuel vapor in an actual PM burner [4-7]. Either liquid or gaseous fuels can be burned by the burner depending on experimental conditions. However, in the present study, the mixture of an axial air and a tracer (olive oil droplets) is used instead of the fuel vapor or gaseous fuel to simulate the fuels flowing through the telescopic end plate PM. Note that the telescopic end plate PM can be moved upstream (to the right-hand side) or downstream with respect to the location of the tangential inlet nozzle by using an external mechanical device (not shown). Therefore, the origin of the coordinate system at $X = 0$ mm is set on the center line of the combustion chamber and at the location where the origin of the coordinate system and the downstream edge of the tangential inlet nozzle is placed on the same plane that is perpendicular with the center line of the combustor. The location of the telescopic end plate PM with respect to the location of the tangential inlet nozzles is defined by an inter-distance X_{PM}, which is the distance between the origin of the coordinate system at $X =$ 0 mm to the exit end of the telescopic end plate PM. In this study, X_{PM} can be varied from -6 mm to 31.75 mm depending on the experimental condition. It will be shown later that it is possible to alter drastically the shape, location and extent of recirculation zones and levels of turbulence intensity generated in the present combustor by alteration of the X_{PM}.

The combustion chamber is also made of an acrylic cylinder, making possible flow visualization and measurements by PIV. For a typical combustion chamber as shown in Fig. 1a, there are four tangential inlet nozzles circumferentially attached to the outside wall of the combustion chamber near the exit of the telescopic end plate PM. The air stream was supplied by the laboratory air compressed line and was divided into two separately metered streams: one was for an axial air for simulating the fuel vapor within the telescopic end plate PM. and the other one was for a tangential air through the four tangential inlet nozzles to impart angular momentum (see section A-A).

Fig. 1b shows various section A-A of the combustion chamber with varying the number of the tangential inlet nozzles N_{inlet} ranging from 1 to 4. With multiple air inlet nozzles, each nozzle was equally spaced along the circumference of the combustion chamber. N_{inlet} is varied in such a way that the inlet velocity is kept constant, whilst the total fuel and air mass flow rate is conserved. This is accomplished by using the inlet nozzle diameter proportional to its actual air mass flow rate at the corresponding N_{inlet}. Therefore, the larger the N_{inlet}, the smaller the air mass flow rate in a nozzle and thus the diameter of the nozzle. In this study, the diameter of the tangential inlet nozzles equal to 7, 5, 4 and 3.5 mm, respectively, are used for N_{inlet} of equal to 1, 2, 3 and 4. For the sake of brevity, the combustion chamber having $N_{inlet} = 1$, 2, 3 and 4, respectively, can be simply identified by the terms Block A, B, C and D as shown in Fig. 1b.

Fig. 1c shows various section A-A for $N_{inlet} = 4$ with variation in an inlet angle ø equal to 45º, 60º, 75º and 90º, respectively, for maximum possible homogeneous mixing of the axial air with tracer and the tangential air. Here, ø is defined as an angle occupied by the tangential direction to the internal surface of the combustion chamber and the tangential direction to the imaginary circle within the chamber. At ø = 0º (Block D in Fig. 1b), however, means a conventional tangential flow, wherein the air inlet nozzles are directed tangentially towards the internal surface of the combustion chamber. Again, the combustion chamber having an inlet angle of ø = 45º, 60º, 75º and 90º, respectively, can be simply identified by Block E, F, G and H as shown in Fig. 1c.

The swirl flow is commonly characterized by two dimensional parameters, a swirl number (*S*) and the Reynolds number (*Re*). The swirl number S is defined as a non-dimensional number representing axial flux of the angular momentum G_ϕ divided by the axial thrust G_X multiplied by the equivalent nozzle radius R [8], as defined by

$$S = \frac{G_\phi}{G_X R} \tag{2}$$

Reynolds number *Re* evaluated at the burner exit conditions and based on the burner exit diameter is also commonly used to characterize flow fields that suffer the swirl flow phenomena, as given by

$$Re = \frac{u_{avg} D}{\nu} \tag{3}$$

Based on the study of Farokhi et al. [9], the swirl number *S*, however, is insufficient to characterize a swirl flow. The swirl number *S* can be inflated or deflated depending on the initial velocity distribution [10]. Therefore, the Reynolds number *Re* is adopted in the present study. The Reynolds number *Re*, based on the average exit velocity (u_{avg}) and geometrical parameter (*D*) is useful particularly when comparing results.

To simulate a condition in an actual combustor [7, 8], the axial air flow rate through the telescopic end plate PM was fixed to about 7.7 L/min, which is equivalent to burning a liquid kerosene fuel with constant firing rate of about 5 kW. However, the tangential air flow rate was varied by adjusting the valve of each tangential air (Fig. 2), which is equivalent to varying an equivalence ratio Φ (defined by a ratio of the stoichiometric air required for complete combustion to the actual air supplied) in the high temperature experiment. In this experiment, however, the total flow rate (axial and tangential air) was typically maintained at a rate to give a nominal *Re* ranging from 2,135 to 4,125, the values of which are equivalent to Φ ranging from 0.8 to 0.4 in the high temperature experiment with a constant firing rate of 5 kW of the liquid kerosene.

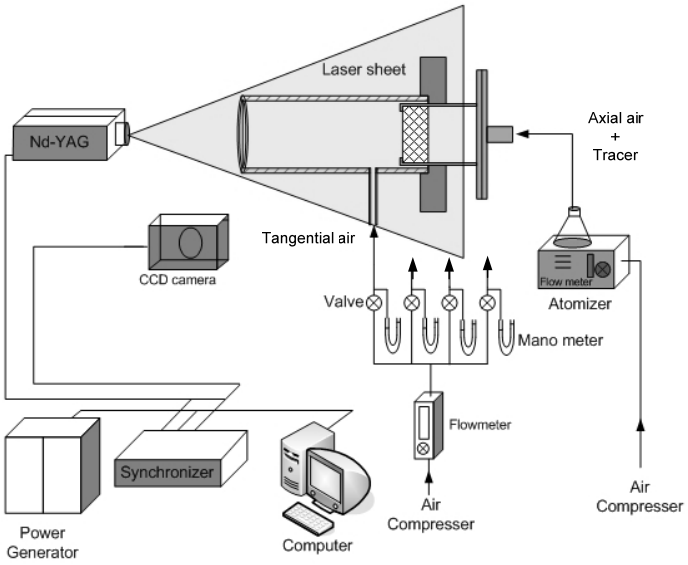

Fig. 2. Schematic diagram of PIV measurements.

2.2 PIV measurement

Fig. 2 shows the PIV system. It consists of a PowerView 2M Plus CCD camera (1600 x 1200 pixels camera with a 28mm F/2.8 Nikon lens and the rate of image acquisition of 15 frames/s), a double pulse Nd:YAG laser (with a pulse duration of 5 ns, a repetition rate of 10 Hz, and an energy of 120 mJ per pulse), a power generator, a host computer, a synchronizer and a droplet atomizer for generating tracer. To enable PIV measurement, the axial air

(from an air compressor) that is supplied into the telescopic end plate PM is seeded with olive oil droplets tracer having a nominal diameter of 1 μm generated by the droplet atomizer. A laser sheet with a wavelength of 532 nm is directed to the transparent combustion chamber with the sheet passing through the combustion chamber axis when measuring the axial velocity component (section A-A in Fig. 1a), while the sheet is perpendicular to the combustion chamber axis at X = -7 mm when measuring the tangential component (Fig. 1a). An interferential filter at 532 nm is placed in front of the CCD camera lens to reject visible light at wavelengths other than 532 nm. The software used for the acquisition and the correlation processing is Insight version 6 from TSI. Tecplot version 10 is used for vector display and additional post processing, such as turbulence visualization. An error associated with this software in pixel units is 0.1 pixels, because the fast Fourier transforms (FFT) is applied for correlation analysis. The interrogation region was 32x32 pixels with a 50% overlap factor. The sub-pixel displacement was estimated by means of Gaussian peak of fitting. With a maximum displacement of 8 pixels, this would correspond to less than 2% uncertainty in final velocity measurement. It was observed that above 150 pairs of images, the mean velocity values and the root mean square (RMS) were constant. Due to the coating of the inner surface of the acrylic combustion chamber with the seeding olive oil droplets during the measurements, acquisition of images was possible only for a specific allowable time interval. Thereafter the acrylic combustion chamber had to be cleaned before any further measurements could be performed.

Mixing performance is described by averaged turbulence intensity TI_{avg}, which is an area averaged value based on the whole-field velocity fields over the target area obtained by PIV. Here, the target area is defined as the area of the rectangle that is surrounded by the dashed lines within the model swirl combustor as shown in Fig. 1a. Therefore, the TI_{avg} is achieved by averaging the local turbulence intensity TI_{ij} over the target area of study as defined by

$$TI_{avg} = \frac{\sum_{i=1}^{i=I}\sum_{j=1}^{j=J} \mathrm{TI_{ij}}}{\mathrm{I \times J}} \tag{4}$$

where i and j, respectively, represent coordinates of the pixel in the X and Y direction, whilst I and J, respectively, represent the numbers of pixels in the X and Y direction within the target area. The TI_{ij} is calculated from the local root mean square of the local fluctuating velocity RMS_{ij} and the corresponding velocity magnitude $\overline{V}_{mag_{ij}}$ at the corresponding local position, as defined by

$$TI_{ij} = \frac{RMS_{ij}}{\overline{V}_{mag_{ij}}} \tag{5}$$

where

$$RMS_{ij} = \sqrt{\overline{u_{ij}'^2} + \overline{v_{ij}'^2}} \tag{6}$$

and

$$\overline{V}_{mag_{ij}} = \sqrt{\overline{u}_{ij}^2 + \overline{v}_{ij}^2} \tag{7}$$

Here, $\overline{u}_{ij}$ and $\overline{v}_{ij}$, respectively, are the local time-averaged velocity in X and Y direction as defined as

$$\overline{u}_{ij} = \frac{\sum_{n=1}^{N} u_{ij}}{N} \tag{8}$$

$$\overline{v}_{ij} = \frac{\sum_{n=1}^{N} v_{ij}}{N} \tag{9}$$

where N is the number of instantaneous local velocity.

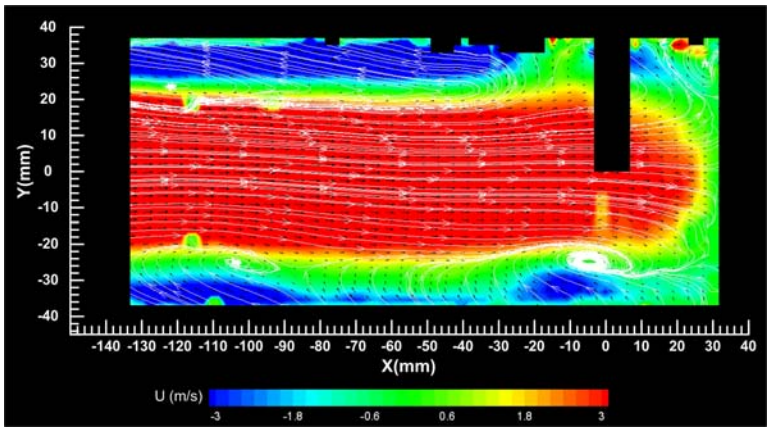

(a) Block A (N_{inlet} = 1)

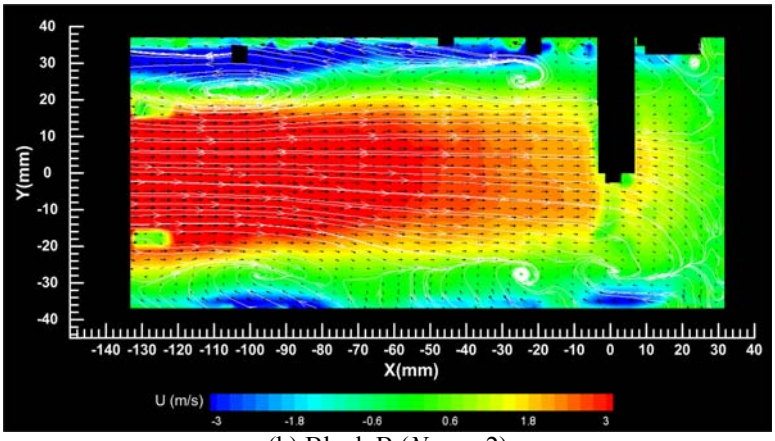

(b) Block B (N_{inlet} = 2)

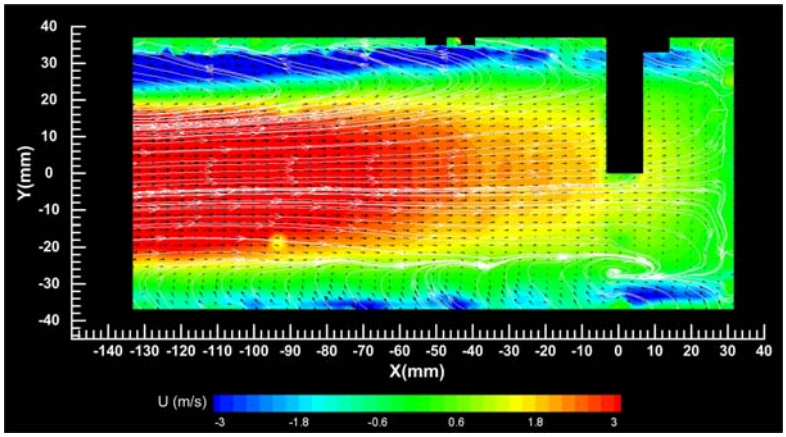

(c) Block D (N_{inlet} = 4)

Fig. 3. Effect of N_{inlet} on velocity vector, streamlines and u-component velocity contour.

3. RESULTS AND DISCUSSION

3.1 Effect of N_{inlet}

Table 1 designates the test model combustors with different parameters of N_{inlet}, ø and X_{PM} at various *Re*. Figs. 3a, 3b and 3c, respectively, show typical effect of N_{inlet} = 1, 2 and 4, which are equivalent to Blocks A, B and D, respectively, on velocity (arrows indicate direction only), streamlines and *u*-component velocity contour at a typical experimental condition of *Re* = 4,125, ø = 0º and X_{PM} = 31.75 mm. The magnitude of the *u*-component velocity within the flow fields is color indexed in unit of m/s. The dark rectangular area at *X* = 0 mm represents a tangential inlet nozzle that tangentially connects with the combustion chamber (Fig. 1a).

General features are observed for the increase in N_{inlet}. As can be seen from Blocks A, B and D as shown in Figs. 3a, 3b and 3c, respectively, owing to greater tangential velocities of the air jets emerging from the tangential inlet nozzles as compared with that of the telescopic end plate PM, the strong centrifugal effects restrain the inlet flow from penetrating towards the center, keeping the inflow closer to the side wall of the combustion chamber and the down flow to the burner exit occuring along the side wall. With a weaker swirl near the center, a backward flow in the central region at the exit is observed in every case because a certain amount of fluid is entrained back into the combustion chamber from farther downstream. The backward flow moves deeper upstream until the telescopic end plate PM is reached, where a stagnation point is established near its surface. Then the backward flow changes its direction and forms a down flow stream along the side wall to the burner exit. A corner recirculation zone (CRZ) is observed near the lower and upper side wall and closer to the tangential inlet nozzle due to the confinement of the swirl flow. The CRZ is important to designers because intense mixing and combustion occur in and near this region, and it exhibits the highest temperature [3]. The backward flow in the central regions indicates the existence of a reverse flow region, which occupies almost entirely the flow regions within the combustion chamber. This implies that the considered swirl flow is strong enough to generate a relatively large radial pressure gradient caused by the centrifugal force effect. This causes a sub-atmospheric low pressure region in the central region of the combustion chamber, which is sufficient to produce the reverse flow. With the reverse flow region, a shear layer is generated in the boundary layer between the inner reverse flow region and the outer down flow stream along the side wall. A clearer impression of the shear layer can be seen from a large difference in the magnitude of the *u*-component velocity contour within the boundary layer, which is color indexed in unit of m/s. The existence of the shear layer in the vicinity of the central region and the CRZ near the side wall of the combustion chamber imply that the flow structures are dominated by convective effects. This greatly enhances the mixing of the fluid streams.

The overall flow field development with respect to N_{inlet} = 1, 2 and 4 as shown in Figs. 3a, 3b and 3c, respectively, can be described as follows. If N_{inlet} = 1 (Block A), a single location of the CRZ exists at the lower side wall near the exit of the inlet nozzle. The burner exhibits an asymmetric feature of the CRZ. This may be attributed to a non-uniformity in the injection flow mainly caused by air inlet nozzles at discrete circumferential locations. With N_{inlet} = 2 (Block B), a better improvement in axisymmetric features of the CRZ can be seen as two locations of the CRZ appear downstream along the lower side wall of the combustion chamber. At N_{inlet} = 3 (not shown), three locations of the CRZ appear along the lower side wall of the combustion chamber with shorter inter-distance between them. It seems that the number of the CRZ corresponds to the number of the inlet nozzle N_{inlet}. Each inlet nozzle may generate its own helical or vortical structure [11, 12] that gyrates around the centerline and persists for some turns before merging with the other helical structure caused by the other inlet nozzle. The multiple locations of the CRZ, however, disappears as N_{inlet} = 4 (Block D) and only a single location of the CRZ is observed near the inlet nozzle. This may be attributed to the merging of the multiple location of the CRZ as mentioned before. The multiple location of the CRZ may cancel each other and be convected downstream, and then dissipated into small-scale eddies. Consequently, the multiple locations of the CRZ disappears.

Fig. 4 shows effect of N_{inlet} on the corresponding TI_{avg} for various *Re* at ø = 0º and X_{PM} = 31.75 mm. At a constant *Re*, as N_{inlet} increases, TI_{avg} linearly increases. This may be attributed to a more uniformly distributed jet velocity across the cross-sectional area of the combustion chamber as N_{inlet} increases. However, TI_{avg} is inversely proportional to *Re*. This may be attributed to the clinging of the tangential flow to the side wall of the combustion chamber. This can cause high viscous dissipation rate at the inner surface of the side wall. The higher the *Re*, the higher the viscous dissipation rate due to the higher centrifugal force.

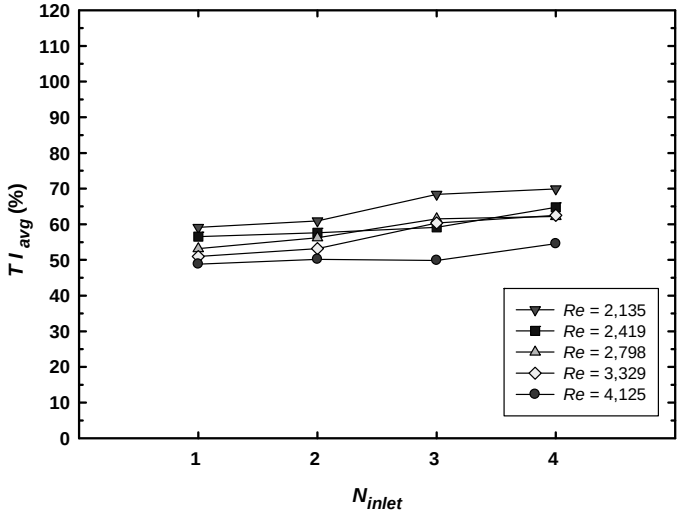

Fig. 4. Effect of N_{inlet} on TI_{avg}.

3.2 Effect of ø

Figs. 5a, 5b and 5c, respectively, show typical effects of a progressive increase of ø = 60º, 75º and 90º, which are equivalent to Blocks F, G and H, respectively, on velocity (arrows indicate direction only), streamlines and *u*-component velocity contour at typical *Re* = 4,125 and X_{PM} = 31.75 mm. General features are observed for the increase in ø from 0º to 90º. The flow is gradually shifted from an edged tangential inlet to a centered tangential inlet and finally to a direct impinging flow at the central axis when ø = 90º. The detailed flow field development with respect to ø, however, can be described as follows.

At 0º ≤ ø < 60º (Block D and E), the burner exhibiting a strong centrifugal effect with enhanced mixing caused by a shear layer and the CRZ within the reverse flow is evident (not shown). However, the CRZ becomes less evident as ø increases due probably to a decrease in the centrifugal effect, which tends to keep the inflow and the generated CRZ closer to the side wall. Moreover, the inflow from each inlet nozzle starts to impinge on each other and thus decrease the centrifugal effect. At ø = 60º (Block F), however, the CRZ appears again at the air inlet nozzle in conjunction with an increase in its size.

At ø = 75º (Block G), however, results in a strong impinging of jets such that a stagnation point is formed near the inlet nozzle at *X* = 2 mm. At this location, a double CRZ is established in conjunction with an enlargement of its size. The double CRZ may be formed by the impinging of jets from nearby inlet nozzles followed by a separation of flows from each inlet nozzle into two streams at the corresponding stagnation point: one is directed to the downstream side of the stagnation point and causes the downstream side CRZ and the other is directed to the upstream side forming the upstream side CRZ. Each CRZ creates its own reverse flow with opposite flow direction. With the double CRZ, the fuel emerging from the exit of the telescopic end plate PM is sucked to mix with the double CRZ with a relatively high velocity as is indicated by a significant increase in the negative *u*-component velocity contour at the fuel exit. The double CRZ is very important for mixing and combustion. Thus, at ø = 75º (Block G) may yield an intense and homogeneous mixing between the fuel emerging from the exit of the telescopic end plate PM and the swirl combustion air emerging from the inlet nozzles through the occurrence of the double CRZ at *X* = 2 mm.

Finally, at ø = 90º (Block H), the inlet flows directly impinge each other at the central axis, forming a stagnation point there. Some of the fluid is reflected from the stagnation point to both the downstream and the upstream sides with some degree of swirl motion which is strong enough to retain the double CRZ. However, each CRZ at each side of the stagnation point is removed from each other with the downstream side CRZ moving farther away to the burner exit with a remarkable enlargement in its size because of its free expansion whereas the upstream side one is still clinging to the surface of the telescopic end plate PM with a relatively small size. Unfavorable positive *u*-component velocity contour is observed at the fuel exit due to the strong impinging of the jets. This can lead to an undesirable combustion within the telescopic end plate PM and damage to it.

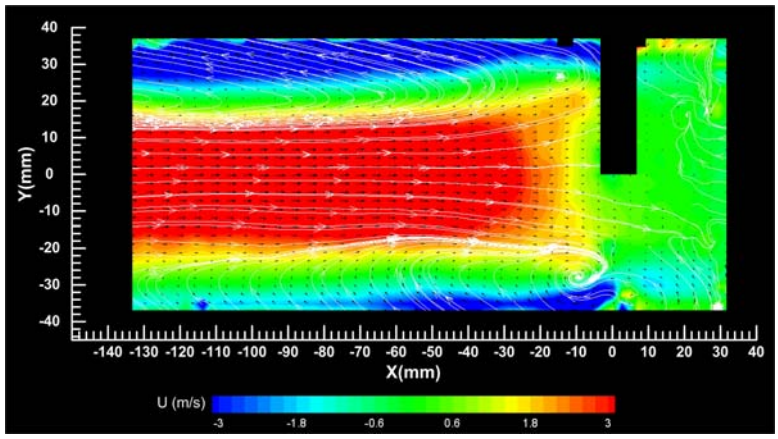

(a) Block F (ø = 60º)

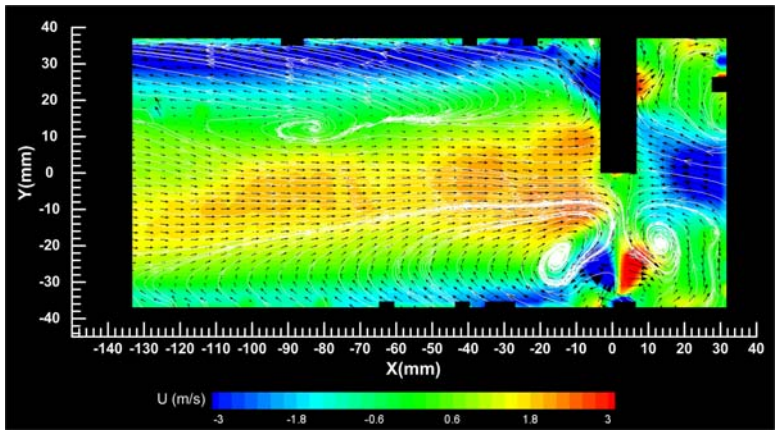

(b) Block G (ø = 75º)

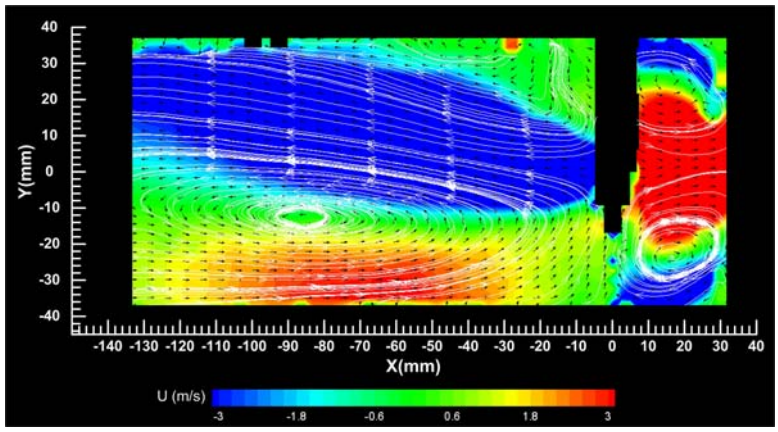

(c) Block H (ø = 90º)

Fig. 5. Effect of *ø* on velocity vector, streamlines and *u*-component velocity contour.

Fig. 6 shows the corresponding TI_{avg} for various *Re* at X_{PM} = 31.75 mm. The abscissa is also scaled by D_{img}/D: a ratio of a diameter of an imaginary circle in which the tangential inlet is in contact with (section A-A in Fig. 1a) and the inside diameter (D = 74 mm) of the combustion chamber. Here, ones can clearly see that the level of TI_{avg} can be significantly improved and optimized by alteration to ø. At a constant *Re*, as ø increases, TI_{avg} increases until a certain value of ø = 75º (Block G) is reached beyond which TI_{avg} sharply decreases owing to an occurrence of a direct impinging of the jets as explained before. TI_{avg} is inversely proportional to *Re* particularly at ø of less than 60º. This may be attributed to the clinging of the tangential flow to the side wall of the combustion chamber at this

relatively low ø. However, at ø larger than 60º, TI_{avg} is proportional to *Re*. As *Re* increases, a slight increase in TI_{avg} is observed.

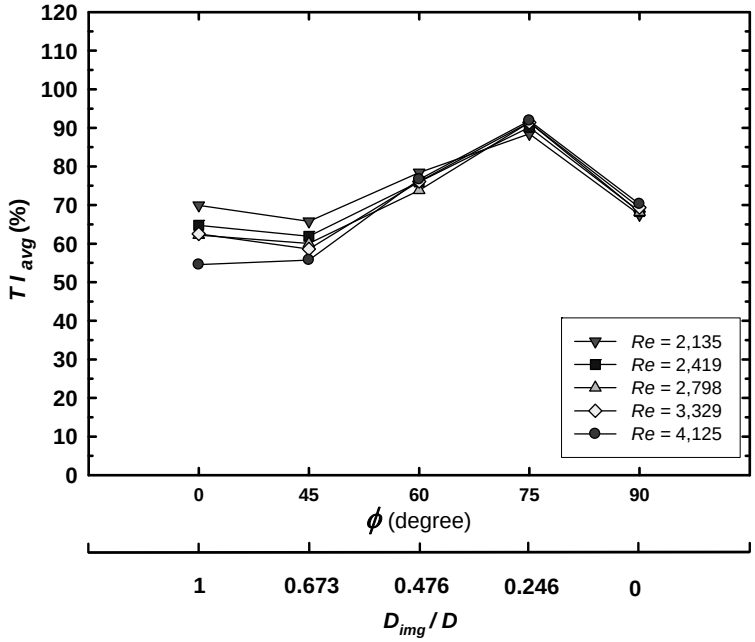

Fig. 6. Effect of ø on TI_{avg}.

3.3 Effect of X_{PM}

Figs. 7a, 7b and 7c, respectively, show typical effects of X_{PM} = 11.75, 0 and -3.5 mm of Block G on velocity, streamlines and *u*-component velocity contour at *Re* = 4,125 and ø = 75º. X_{PM} strongly affects the swirl flow field. At X_{PM} = 31.75 mm (Fig. 5b), the burner exhibiting the maximum TI_{avg} with the double CRZ is evident. As X_{PM} is decreased to X_{PM} = 21.75 mm (not shown), however, the double CRZ become less evident due probably to the jet impinging on the telescopic end plate PM. As X_{PM} is further decreased to X_{PM} =11.75 mm (Fig. 7a), the double CRZ completely disappears, leaving only a single CRZ at the corners of the telescopic end plate PM together with a stagnation plane located at X = 2 mm.

At X_{PM} = 0 mm (Fig. 7b), however, it results in both the CRZ being located at the upper corner of the telescopic end plate PM in conjunction with an appearance of a large single central toroidal recirculation zone (CTRZ) near the centerline at some distance downstream from the telescopic end plate PM. It is important to note that at this location of X_{PM} = 0 mm the telescopic end plate PM is marginally located at the same level of the downstream edge of the inlet nozzle (X = 0 mm). Therefore, the centered tangential flow of the air begins transforming to a swirling annulus flow of air, which covers the fuel exit at the center of the telescopic end plate PM. Therefore, a vortex breakdown can be generated in the downstream of the fuel exit provided that the swirling annulus air jet velocity is high enough. As is the case for the present study, both CRZ and CTRZ are generated, indicating the characteristics of the high swirl phenomena despite their asymmetry due probably to complex fluid dynamic characteristics. The CTRZ plays an important role in mixing and flame stabilization by providing a continuous heat source of recirculated combustion products and a reduced velocity region where flame speed and flow velocity can be matched [3]. Moreover, an interesting phenomena can be expected at this location of X_{PM} = 0 mm (Fig. 7b) if combustion occurs. Premixing of fuel and air is not allowed to take place because the air inlet nozzles are blocked by the leading edge of the telescopic end plate PM. Rather, mixing of fuel and air is controlled by diffusion and thus, a diffusion (non-premixed) flame can be expected. Therefore, either a premixed or a non-premixed free flame can be made by adjusting X_{PM} of the present burner system provided that a certain threshold of swirl strength or fuel and air flow rate is reached [10]. This also implies a possibility of a premixed or a non-premixed submerged flame within a porous medium burner (PMB) if, instead of a free space, the PMB is installed downstream of the telescopic top plate PM. Further decrease in X_{PM} to -3.5 mm (Fig. 7c) results in a more evident corner CRZ with a large,

asymmetric CTRZ due probably to an improvement in the swirling annulus flow of air. This can confirm that the swirl flow combustion with controlled flow field using telescopic end plate PM is possible.

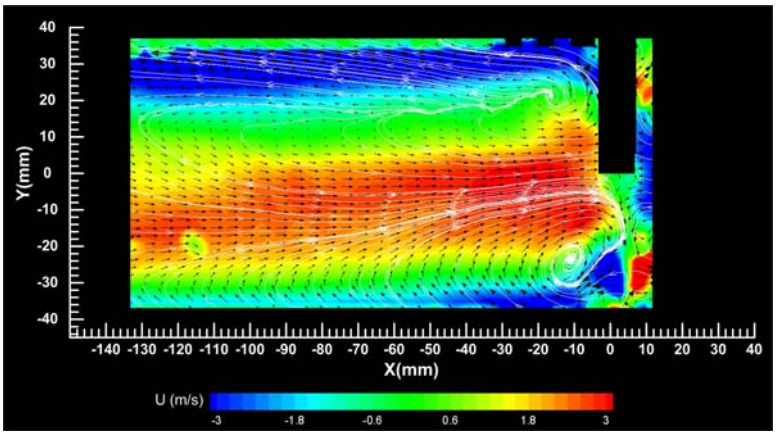

(a) X_{PM} = 11.75 mm

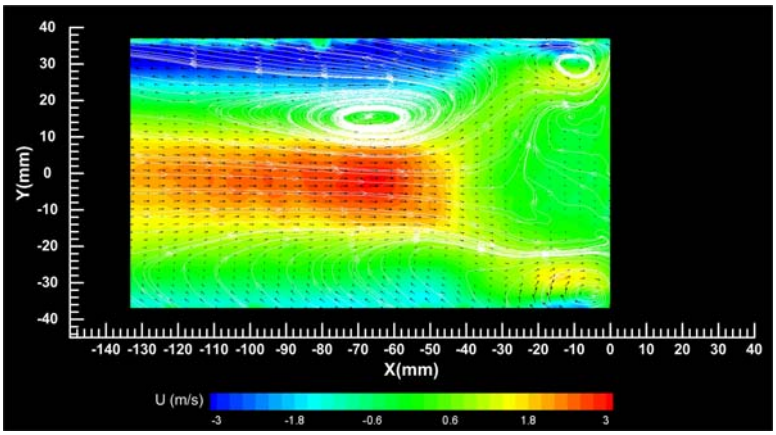

(b) X_{PM} = 0 mm

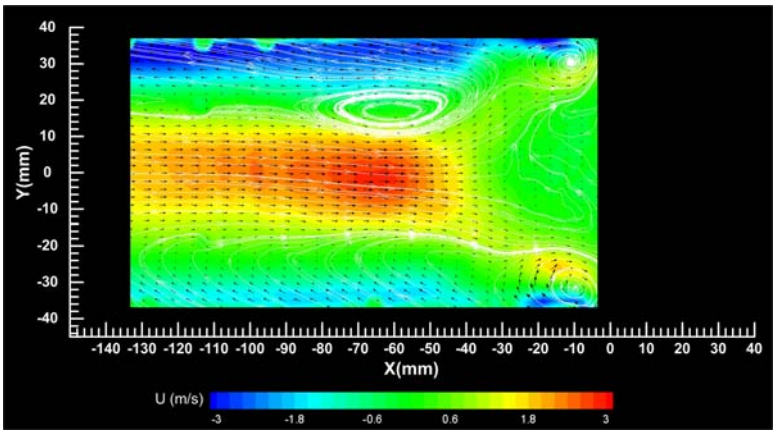

(c) X_{PM} = −3.5 mm

Fig. 7. Effect of X_{PM} (Block G) on velocity vector, streamlines and u-component velocity contour.

Fig. 8 shows the corresponding TI_{avg} in an axial and a tangential direction at various Re ranging from 2,135 to 4,125 of Block G. The abscissa is also scaled by ratio of X_{PM} to its allowable maximum value of X_{PMmax} = 31.75 mm. The measurement of the tangential TI_{avg} is performed at a typical burner cross section at X = -7 mm as shown in Fig. 1a so as to study the relationship between the tangential TI_{avg} and the axial one. At any constant values of Re, as X_{PM} is

decreased from 31.75 to -3.5 mm, it has a negligible effect on both the axial and the tangential TI_{avg} until a value of X_{PM} = 11.75 mm is reached below which both the axial and the tangential TI_{avg} significantly change with X_{PM} and *Re*. At X_{PM} of smaller than 11.75 mm, the axial TI_{avg} shows a decreasing trend (with an exception at relatively low *Re* = 2,135), whereas the tangential TI_{avg} drastically increases, indicating an occurrence of the above mentioned annulus flow wherein the air from the inlet nozzles is forced to flow tangentially along the side wall. Both axial and tangential TI_{avg} are inversely proportional to *Re* because of clinging of the tangential flow to the side wall.

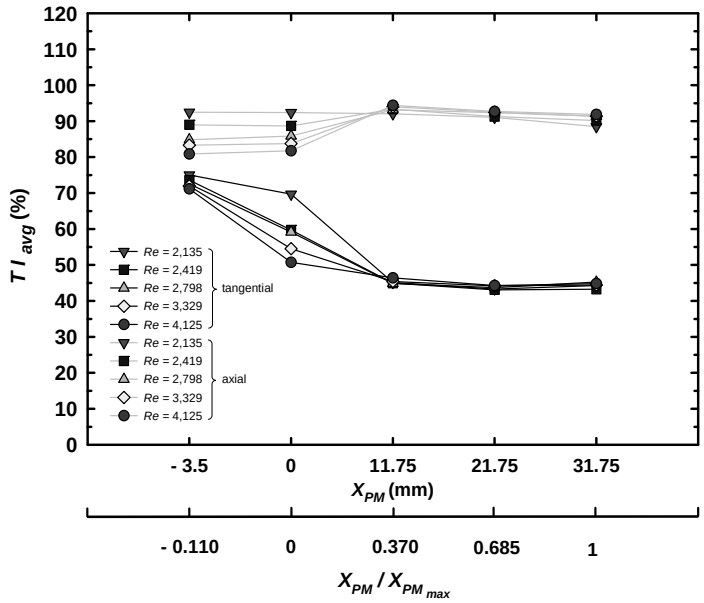

Fig. 8. Effect of X_{PM} (Block G) on TI_{avg}.

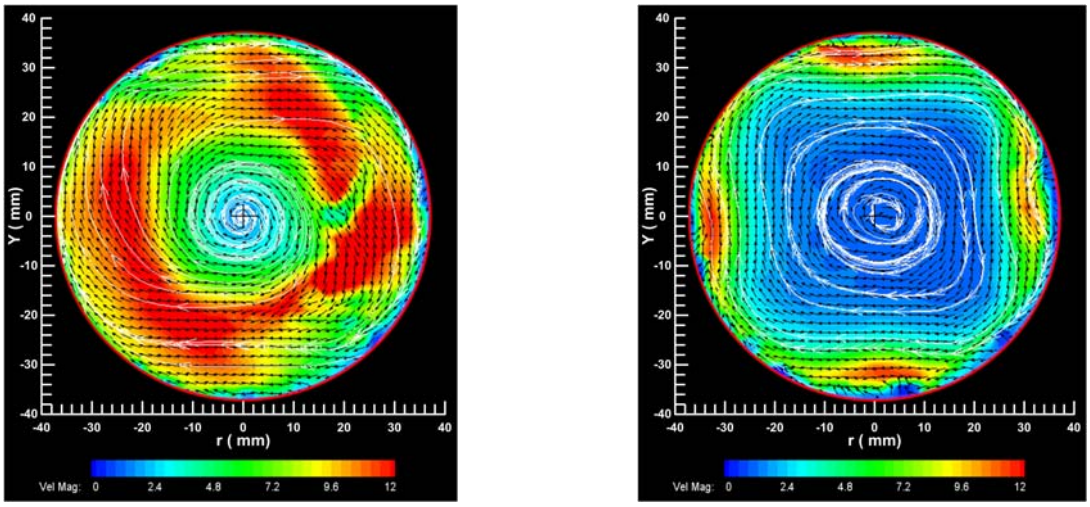

(a) X_{PM} = 31.75 mm (b) X_{PM} = 0 mm

Fig. 9. Effect of X_{PM} (Block G) on velocity vector, streamlines and *w*-component velocity contour.

In order to confirm the annulus flow, a comparison between two typical tangential velocity (or *w*-component velocity) contours at two different locations of X_{PM} = 31.75 mm and X_{PM} = 0 mm were conducted for Block G as shown in Fig. 9. At X_{PM} = 31.75 mm (Fig. 9a) a relatively high tangential velocity contour is taken place in a relatively wide area ranging from the mid-point of the burner radius to the burner side wall. At X_{PM} = 0 mm (Figs. 9b), however, the high tangential velocity contour is concentrated in the area near the side wall of the combustion chamber, indicating an annulus flow.

Table 1: Designations of test model combustors with different parameters of N_{inlet}, ø, and X_{PM} at various *Re*

Designation	N_{inlet}	ø (degree)	X_{PM} (mm)	*Re*
Block A	1	0	31.75	2,135 - 4,125
Block B	2	0	31.75	2,135 - 4,125
Block C	3	0	31.75	2,135 - 4,125
Block D	4	0	31.75	2,135 - 4,125
Block E	4	45	31.75	2,135 - 4,125
Block F	4	60	31.75	2,135 - 4,125
Block G	4	75	31.75	2,135 - 4,125
Block H	4	90	31.75	2,135 - 4,125
Block G	4	75	21.75	2,135 - 4,125
Block G	4	75	11.75	2,135 - 4,125
Block G	4	75	0	2,135 - 4,125
Block G	4	75	-3.5	2,135 - 4,125

4. CONCLUSIONS

A non-reacting, model swirl combustor equipped with a telescopic end plate PM has been presented. Various important parameters controlling flow fields and mixing have been investigated using PIV to characterize the flow fields and optimize mixing performance of the model combustor. The following conclusions can be drawn from the studied results.

1. The number of the tangential inlet nozzles N_{inlet} moderately affects the flow field and the average turbulence intensity TI_{avg}.
2. The inlet angle ø significantly affects both the flow field and the average turbulence intensity TI_{avg}. The study revealed an optimum burner configuration with ø = 75º and N_{inlet} = 4 (Block G).
3. The inter-distance X_{PM} has a large scale effect on both flow fields and mixing performance. Within the appropriate range of the X_{PM} studied, it strongly affects the flow fields without significant sacrifice in the decrease in TI_{avg}. A threshold value of X_{PM} = 0 mm was obtained, at which the swirl flow field starts shifting from the centered tangential flow with the formation of CRZ (corner recirculation zone) to the annular flow with the generation of both the CRZ and the CTRZ (central toroidal recirculation zone).
4. The study implies a possibility of a premixed or a non-premixed submerged flame within an actual PM burner if, instead of a free space, a packed bed of PM is installed downstream of the telescopic end plate PM.

5. ACKNOWLEDGEMENTS

This work was supported by the Higher Education Research Promotion and National Research University Project of Thailand, Office of the Higher Education Commission.

REFERENCES

[1] Swithenbank, J. and Chigier, N.A. Vortex mixing for supersonic combustion, paper presented in the 12th Symposium (International) on Combustion, The Combustion Institute, 1970, pp. 1153-1162.

[2] Chigier, N.A. and Chervinsky, A. Aerodynamic study of turbulent burning free jets with swirl, paper presented in the 11th Symposium (International) on Combustion, The Combustion Institute, 1967, pp. 489-499.

[3] Gupta, A.K., Lilley, D.G. and Syred, N. Swirl Flows, ISBN: 0-85626-175-0, 1984, Abacus Press, Cambridge, Massachusetts, USA.

[4] Jugjai, S., Wongpanit, N., Laoketkan, T. and Nokkaew, S. Experimental study on combustion of liquid fuels by a porous medium, Experimental Thermal and Fluid Science, Vol. 26(1), 2002, pp. 15-23.

[5] Jugjai, S. and Polmart, N. Enhancement of evaporation and combustion of liquid fuels through porous media, Experimental Thermal and Fluid Science, Vol. 27(8), 2003, pp. 901-909.

[6] Jugjai, S. and Pongsai, C. Liquid fuel-fired porous burner, Combustion Science and Technology, Vol. 179(9), 2007, pp. 1823-1840.

[7] Jugjai, S. and Phothiya. C. Liquid fuel-fired porous combustor-heater, Fuel, Vol. 86(7-8), 2007, pp. 1062-1068.
[8] Beer, J.M. and Chigier, N.A. Combustion aerodynamics, ISBN: 0-85334-513-9, 1972, Applied Science, London.
[9] Farokhi, S., Taghavi, R. and Rice, E.J. Effect of initial swirl distribution on the evolution of a turbulent jet, Journal of American Institute of Aeronautics and Astronautics, Vol. 27(6), 1989, pp. 700-706.
[10] Toh, I.K., Honnery, D. and Soria, J. Axial plus tangential entry swirling jet, Experiments in Fluids, Vol. 48(2), 2010, pp. 309-325.
[11] Shtork, S.I., Cala, C.E., Fernandes, E.C. and Heitor, M.V. Coherent helical structures in swirl flows, Technical Physics Letters, Vol. 31(8), 2005, pp. 660-662.
[12] Huang, Y. and Yang, V. Effect of swirl on combustion dynamics in a lean-premixed swirl-stabilized combustor, Proceedings of the Combustion Institute, Vol. 30(2), 2005, pp. 1775-1782.